Integrated Surface-Airspace Model of Airport Departures

Sandeep Badrinath*, Max Z. Li†, and Hamsa Balakrishnan‡

Massachusetts Institute of Technology, Cambridge, Massachusetts, 02139

The significant growth in air traffic over the past few decades has led to increased congestion at major airports. Departure metering strategies to mitigate congestion require good models of operations at the airport, as well as in the surrounding terminal airspace. While runways have traditionally been considered the sole capacity bottleneck in the air transportation system, large airports can exhibit multiple points of congestion, both on the surface, and in the terminal-area. This paper presents an integrated surface-airspace model of aircraft departure operations from pushback to the final departure fix, when the flight leaves the terminal-area. The airport surface is represented as a queuing network to capture congestion at multiple locations such as ramp, taxiways, and runways. The terminal departure airspace is modeled considering various factors such as runway configurations, standard departure procedures, weather, and en route traffic. The proposed modeling approach is illustrated for Charlotte Douglas International Airport (CLT), the testbed for NASA's Airspace Technology Demonstration 2 (ATD-2) program. The model is evaluated on its ability to accurately predict various transit times, both on the surface and in the terminal-area.

I. Introduction

Airport surface congestion, and the resulting delays, are occur when the demand for aircraft operations exceeds the available capacity. In addition to passenger dissatisfaction, delays are known to lead to increased fuel burn and emissions. Increasing the capacity of an airport by adding physical infrastructure (runways, for example) tends to be both time- and capital-intensive, and even infeasible [1, 2]. As a result, there is interest in near-term operational changes to increase airport capacity [3, 4], as well techniques to manage demand. Economic incentives such as congestion pricing have been proposed to regulate the scheduled demand for constrained resources, but often encounter policy barriers [5]. These factors motivate the development of more tactical, operational approaches that alleviate airport congestion by efficiently utilizing currently available capacity.

Departure metering as a means to mitigate the adverse impacts of congestion has been the focus of considerable research [6–13]. The key idea behind departure metering is to regulate the pushback of departures from their gates in

---

*Graduate student, Department of Aeronautics and Astronautics, Massachusetts Institute of Technology, AIAA student member.

†Graduate student, Department of Aeronautics and Astronautics, Massachusetts Institute of Technology, AIAA student member.

‡Associate Professor, Department of Aeronautics and Astronautics, Massachusetts Institute of Technology, AIAA Associate Fellow.

order to avoid excessive congestion, while at the same time taking care to maintain runway utilization. Although the specifics of departure metering algorithms can vary, most require a model of departure operations, and the prediction of taxi-out times [9, 14, 15]. In addition to their use in the development of departure metering algorithms, models of surface operations can be used to characterize airport operations, analyze new and existing procedures, and evaluate the environmental impacts of airport operations.

Models of the airport surface have been broadly described as microscopic, mesoscopic, or macroscopic, based on their level of fidelity [7, 16]. *Microscopic* models (for example, NASA's Surface Operations Simulator and Scheduler (SOSS), or commercial tools such as SIMMOD), specify the dynamics for each aircraft as well as the detailed airport layout [17]. Model predictions require the simulation of individual aircraft trajectories, yielding high-fidelity results. The main disadvantage of microscopic models is that the predictions can be computationally intensive (especially in the presence of uncertainty), simulations can 'gridlock' requiring manual intervention and resolution, and the adaptation of models to new airports and operating conditions can be challenging. In *mesoscopic* models, the taxiways and runways are represented by links with associated travel-time and service time distributions, leading to lower fidelity compared to the microscopic model [9, 13]. The identification of these models requires the availability of large amounts of surface trajectory data, in order to estimate transit time distributions of individual links under different conditions. Finally, we refer to queuing models, and other aggregate statistical models, as being *macroscopic* in nature [16, 18, 19]. These models are based on aggregate variables such as queue lengths and travel times over relatively large parts of the airport (as opposed to individual aircraft or taxiway links). Despite their lower fidelity, their simplicity makes these models amenable to fast-time simulations and easy to integrate into decision support tools.

Airport surface queuing models have traditionally assumed that congestion occurs exclusively near the departure runway [14, 16, 18, 20]. While this is true at some airports, at others with complex layouts such as Charlotte Douglas International airport (CLT), congestion can occur at multiple locations, both on the surface and in the terminal-area. This has motivated research into integrating surface and terminal-area operations to reduce congestion [11, 21–23]. Moreover, arrivals and departures interact and even compete for airport resources such as taxiways. This paper illustrates that at such airports, multistage congestion can be best represented by a queuing network.

In this paper, we present an integrated surface-airspace model for the departure process that predicts the traversal of flights from their departure gates to their final departure fixes. The airport surface is modeled as a queuing network, in order to account for congestion at multiple locations, considering both departures and arrivals. The model enables the prediction of different queue lengths at the airport, as well as taxi-out times for departures and taxi-in times for arrivals. In order to capture the nonstationarity of queues due to time-varying capacity and demand, we present a fluid flow model, that results in a computationally tractable nonlinear ordinary differential equation (ODE) representation of the queuing dynamics. The resulting model is expected to be amenable to the design of efficient congestion control strategies using techniques from optimal control. The terminal airspace is modeled considering standard departure

2

procedures and transition routes. We investigate the influence of traffic density, weather and runway configuration on departure and transition airspace transit times. The proposed model is expected to provide better situational awareness for air traffic controllers, and improve surface traffic management programs, by considering congestion both on the surface and in the airspace. Finally, the model can be used to evaluate the benefits of departure metering algorithms, even in the presence of uncertainty [24].

II. Background

A. Charlotte Douglas International Airport (CLT)

We demonstrate the application of our modeling approach to the case of Charlotte Douglas International Airport (CLT). CLT is a critical node in the United States (US) National Airspace System (NAS), and is a major hub for American Airlines. It handled more than 1,400 flights/day and 44.4 million passengers in 2016, and is the 7th busiest airport in the world, in terms of aircraft movements [25, 26].

The CLT airport layout is notable because of the significant extent of its ramp operations, as well as the considerable interactions between arrivals and departures on the surface [27]. Beyond the airport surface, the terminal airspace around CLT is also a dynamic environment located in close proximity to the intersection of ZTL, ZDC, and ZJX air route traffic control centers (ARTCCs). Furthermore, the Charlotte metroplex – an area of the NAS containing multiple busy airports, resulting in complex airspace geometries, usages, and requiring multileveled coordination [28] – has been identified by the FAA to be of significant interest. For the aforementioned reasons, CLT is a key test site for the FAA's Next Generation Air Transportation System (NextGen) capabilities, including NASA's Airspace Technology Demonstration 2 (ATD-2) program, of which departure metering is a key element [23, 29–31].

B. Data sources

We adopted a data-driven approach to airport characterization and identification of model parameters, using a range of operational data sources. Flight tracks on the surface were obtained from the Airport Surface Detection Equipment, Model X (ASDE-X) system [32]. It included the latitude, longitude, velocity, heading, aircraft type and aircraft ID for each flight, at a 1 Hz sampling rate. The actual pushback, in-air (wheels-off), landing (wheels-on) and in-gate times, and gate assignments, were obtained from OAG data [25]. The meteorological conditions (MC) at the airport (Visual or VMC/ Instrument or IMC) were obtained from the FAA's ASPM database [33]. The surface data was obtained for May-July 2015 and May-June 2016. The selection of these months for the analysis was based on data availability, as well as the increased traffic demand experienced during the summer months.

Airborne flight tracks for May-June 2016 were obtained from FlightAware [34]. These tracks include latitude, longitude, heading, altitude and ground speed, and are fused from radar data feeds via the Enhanced Traffic Management System (ETMS), surface data feeds via ASDE-X, and an ad-hoc network of Automatic Dependent Surveillance-Broadcast

(ADS-B) and multilateration (MLAT)-enabled receivers. The sampling time ranges from 30 s within the terminal airspace to 2 min in the en route phase.

III. Queuing network model

The proposed queuing network model is based on a point-wise stationary fluid flow approximation [35, 36]. The model is a continuum approximation to the discrete queuing problem, derived by combining results from steady state queuing theory with the flow conservation principle. The model for a single queue is presented first, and then extended to a network of queues.

A. Model of a single queue

Let $x(t)$ represent the average number of customers in the queue at time t. Let $f_i(t)$ and $f_o(t)$ represent the in-flow and out-flow from the queue at time t. All the quantities are ensemble averages at a particular time instant. From the flow conservation principle, we have:

$$\dot{x}(t) = -f_o(t) + f_i(t). \tag{1}$$

Let $\lambda(t)$ and $\mu(t)$ denote the average arrival rate and service rate, respectively, at time t. Assuming that there are no constraints on the queue length, we have $f_i(t) = \lambda(t)$. For the out-flow, we can write $f_o(t) = \mu(t)\rho(t)$, where $\rho(t)$ is the average utilization of the server. The queue dynamics therefore takes the form

$$\dot{x}(t) = -\mu(t)\rho(t) + \lambda(t). \tag{2}$$

The average utilization, $\rho(t)$, is approximated by a function, $G(x(t))$, which needs to satisfy the following properties: (a) $G(0) = 0$ and $G(\infty) = 1$; and (b) $G(x)$ is strictly concave and non-negative $\forall x \in [0, \infty)$, in order to represent congestion. The dynamics for $x(t)$ can then be rewritten in terms of $G(x)$ as:

$$\dot{x}(t) = -\mu(t)G(x) + \lambda(t), \quad x(0) = x_0. \tag{3}$$

The expression for $G(x)$ is obtained by matching the steady-state number of customers in the system. Assuming a Poisson arrival process, the Pollaczek-Khinchine formula (4) provides an expression for the mean number of customers (x_s) at steady state [37], namely,

$$x_s = \rho + \frac{\rho^2(1 + C_v^2)}{2(1 - \rho)}. \tag{4}$$

4

Here, C_v is the coefficient of variation of the service time distribution. Expressing ρ in terms of x_s, we get:

$$\rho = \frac{x_s + 1 - \sqrt{x_s^2 + 2C_v^2 x_s + 1}}{1 - C_v^2}. \tag{5}$$

Using the fact that $G(x)$ is an approximation for ρ, we can write

$$\rho(t) \approx G(x) = \frac{x + 1 - \sqrt{x^2 + 2C_v^2 x + 1}}{1 - C_v^2}. \tag{6}$$

The function $G(x)$ is further approximated by $Cx/(1 + Cx)$, in order to obtain a simpler expression for the queue dynamics. The parameter C is determined through the following minimization:

$$\min_C \int_0^{x_m} \left(G(x) - \frac{Cx}{(1 + Cx)} \right)^2 dx. \tag{7}$$

Here, x_m denotes the maximum queue size expected in the system. A comparison between the approximation for $G(x)$ and its actual value for some representative values of the parameters ($C_v = 0.67, x_m = 15, C = 1.23$) is shown in Fig. 1. We can see a good match between the approximation and the actual value. Using the above approximation for $G(x)$, we get an ODE for the evolution of the mean queue length:

$$\dot{x}(t) = -\mu(t) \frac{C(t)x(t)}{1 + C(t)x(t)} + \lambda(t) \tag{8}$$
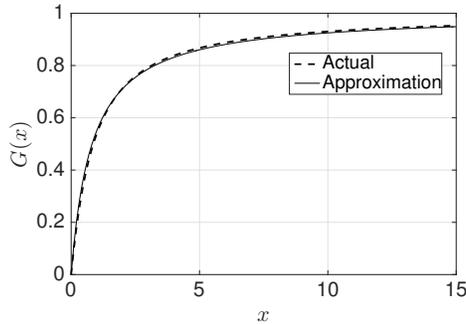
Fig. 1   Comparison between the approximation for G(x) and the actual value.

1. Extension to multiclass queues

We could extend the model to handle multiple classes of customers (aircraft in our case) [35]. Let $i = 1, 2, .. l$ be the different class of customers in the system, x_i being the number of customers of class i in the queue buffer. The

evolution of total number of customers in the queue ($x_T = \sum_{i=1}^{l} x_i$) can be obtained using Eq. (8):

$$\dot{x}_T = -\mu \frac{Cx_T}{1 + Cx_T} + \lambda \tag{9}$$

The fraction of service used by each class is assumed to be proportional to the fraction of customers of that particular class in the queue buffer. Using this assumption, the evolution of mean queue length of a particular class i is given by:

$$\dot{x}_i = -\mu \frac{Cx_T}{1 + Cx_T} \frac{x_i}{x_T} + \lambda \tag{10}$$

$$\dot{x}_i = -\mu \frac{Cx_i}{1 + Cx_T} + \lambda \tag{11}$$

B. Extension to a queuing network

The single queue model can be extended to multiple queues using the flow conservation principle: The output of one queue becomes the input to the second queue if they are connected. Let R be the routing matrix, with elements r_{ij} representing the fraction of customers joining queue j after being served by server i. Let λ_i be the exogenous input into queue i with mean service rate μ_i. The dynamics of the mean queue length for each queue in the network is given by:

$$\dot{x}_i = -\mu_i \frac{C_i x_i}{1 + C_i x_i} + \lambda_i + \sum_j \mu_j \frac{C_j x_j}{1 + C_j x_j} r_{ji} \tag{12}$$

We could additionally use (11) to handle multiple classes of customers in the network.

C. Incorporation of time-delays

Another aspect that arises in many realistic queuing networks are time-delays due to propagation. Note that the propagation delay does not include the wait time in the queue. Let τ_{ij} be the propagation time (travel time) from server i to j. Then, the mean queue length is given by the following delay differential equation:

$$\dot{x}_i = -\mu_i \frac{C_i x_i}{1 + C_i x_i} + \lambda_i + \sum_j \mu_j(t - \tau_{ji}) \frac{C_j(t - \tau_{ji})x_j(t - \tau_{ji})}{1 + C_j(t - \tau_{ji})x_j(t - \tau_{ji})} r_{ji}(t - \tau_{ji}) \tag{13}$$

IV. Queuing network model for the airport surface: North-Flow configuration

We apply the queuing network model developed in the previous section to the case of airport surface operations. CLT operates under two broad runway configurations: North-Flow and South-Flow. The runway configuration refers to the set of runways used at the airport for an extended period of time, and they are determined based on a number of factors such as weather and traffic demand. We first present a model for the North-Flow configuration, and later adapt it

to the South-Flow configuration.

The North-Flow configuration handled about 56% of the traffic at CLT in 2016 [33]. Fig. 2(a) shows the airport layout of CLT, along with a snapshot of aircraft positions, departing flights represented by black triangles and arriving ones represented by white triangles. Three parallel runways (36L, 36C and 36R) are actively used in this particular configuration. All three runways are used for landings, whereas only 36C and 36R are used for takeoffs. The arrival and departure runways are indicated using green and red arrows in Fig. 2(a). The figure also shows queues being formed in the ramp area, near the runway crossing, and at the departure runways.

(a) Airport layout with a snapshot of aircraft positions.

(b) Queuing network representation.
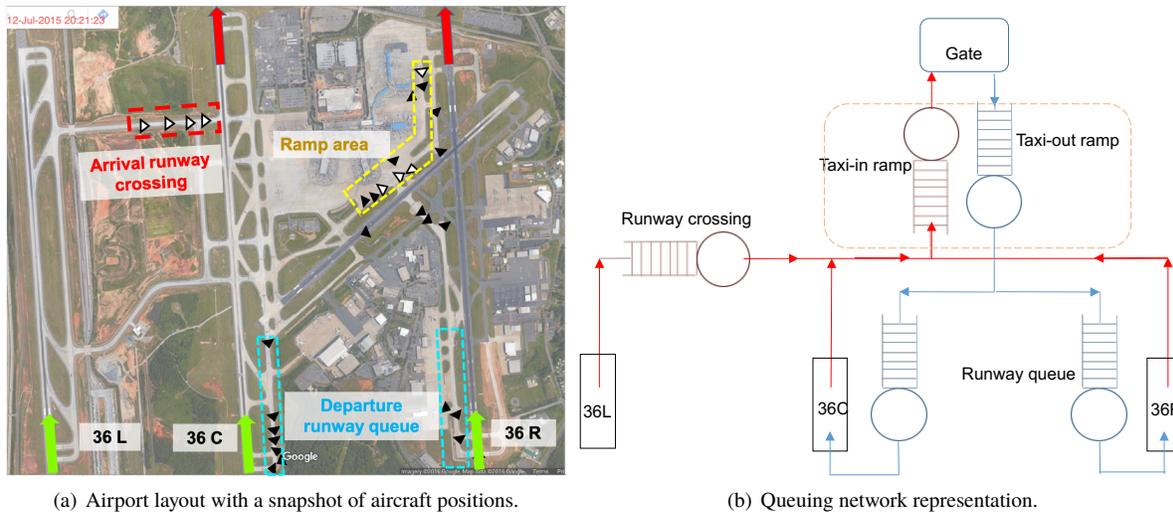
Fig. 2 **The airport layout and queuing network representation for CLT surface operations in the North-Flow configuration.**

To account for congestion at multiple locations on the surface, the movement of traffic can be represented as a queuing network shown in Fig. 2(b). This network is comprised of five queues, three for taxi-out flight movements (shown in blue) and two for the taxi-in flight movements (shown in red). The departures pass through a taxi-out ramp queue and one of two runway queues, depending on their runway assignment. Flights landing on the leftmost runway (36L) pass through a runway crossing queue and taxi-in ramp queue, whereas flights landing on the other runways just pass through the taxi-in ramp queue. Once we have modeled the queue dynamics, the taxi time can be estimated as the sum of the unimpeded time (travel time without any delay) and the wait times in queues.

We adapt the generic queuing network model described in Section III. Although the model is deterministic, it captures the dynamic behavior of non-stationary queues, and allows us to predict taxi times for both arrivals and departures. We validate our model in terms of predicting the queue sizes on the airport surface as well as the taxi times, using operational data from CLT.

A. Queuing network model

From Fig. 2(b), we see that aircraft taxiing-out travel through the taxi-out ramp queue and the departure runway queue. An aircraft is said to be in the taxi-out ramp queue if its travel time after pushing back from the gate has exceeded the unimpeded gate to spot time, but is yet to exit the ramp area (the *spots* are the exit points in the ramp area leading to the active movement area). The customers (aircraft) in the taxi-out ramp queue are categorized into two classes depending on the runway assignment. Let $x_{d,si}$ be the number of flights in the ramp queue heading to runway i ($i = 1, 2, 3$ corresponds to runway 36L, 36C and 36R, respectively). The departure ramp queue is served by a single server of mean service rate $\mu_{d,s}$. The fraction of service used by each class of customers (aircraft) is assumed to be proportional to the fraction of customers of that particular class in the queue. The input to the system is the pushback rate ($u_{d,ri}$) at the gate to each runway i. The total time taken by a flight to exit the ramp area includes the unimpeded travel time from the gate to the spot, and the wait time in the ramp queue. The unimpeded time varies by gate-spot combination, depending on the distance between them. For simplicity, we consider a weighted average unimpeded time over all gate-spot combinations, with the weights proportional to the frequency of operation. The average unimpeded time from gate to spot is denoted by t_1. The unimpeded travel time leads to delay in the ramp queue dynamics, i.e. if the pushback rate at the gate is $u_{d,ri}(t)$, then the arrival rate into the queue is $u_{d,ri}(t - t_1)$. Therefore, the dynamics of the taxi-out ramp queue is given by

$$x_{d,s}(t) = x_{d,s2}(t) + x_{d,s3}(t) \tag{14}$$

$$\dot{x}_{d,s2}(t) = -\mu_{d,s}(t)\frac{C_{d,s}(t)x_{d,s2}(t)}{1 + C_{d,s}x_{d,s}(t)} + u_{d,r2}(t - t_1) \tag{15}$$

$$\dot{x}_{d,s3}(t) = -\mu_{d,s}(t)\frac{C_{d,s}(t)x_{d,s3}(t)}{1 + C_{d,s}x_{d,s}(t)} + u_{d,r3}(t - t_1) \tag{16}$$

The two runway queues are assumed to be independent of each other. Let $x_{d,ri}$ be the number of aircraft in the ith runway queue, and $\mu_{d,ri}$ be the mean service rate of the departure runway server. An aircraft is said to be in the departure runway queue if its travel time after exiting the ramp has exceeded the unimpeded time from spot to runway, but it is yet to take off. The output of the ramp queue is the input to the runway queue delayed by time t_2, where t_2 is the average unimpeded time from spot to runway. The dynamics of the runway queue is then of the form

$$\dot{x}_{d,r2}(t) = -\mu_{d,r2}(t)\frac{C_{d,r2}x_{d,r2}(t)}{1 + C_{d,r2}x_{d,r2}(t)} + \mu_{d,s}(t - t_2)\frac{C_{d,s}(t - t_2)x_{d,s2}(t - t_2)}{1 + C_{d,s}(t - t_2)x_{d,s}(t - t_2)} \tag{17}$$

$$\dot{x}_{d,r3}(t) = -\mu_{d,r3}(t)\frac{C_{d,r3}x_{d,r3}(t)}{1 + C_{d,r3}x_{d,r3}(t)} + \mu_{d,s}(t - t_2)\frac{C_{d,s}(t - t_2)x_{d,s3}(t - t_2)}{1 + C_{d,s}(t - t_2)x_{d,s}(t - t_2)}. \tag{18}$$

Flights landing on 36L have to pass through a runway crossing queue before entering the ramp area. Let $u_{a,ri}$ be the landing rate (of arrivals) on the ith runway. The input to the runway crossing queue is the landing rate on runway

36L, with an associated delay (t_3) accounting for the travel time to reach the runway crossing queue from the point of touchdown. The dynamics of the runway crossing queue length ($x_{a,r1}$) are given by

$$\dot{x}_{a,r1}(t) = -\mu_{a,r1}(t)\frac{C_{a,r1}x_{a,r1}(t)}{1 + C_{a,r1}x_{a,r1}(t)} + u_{a,r1}(t - t_3). \tag{19}$$

An aircraft is defined to be in the taxi-in ramp queue if it has entered the ramp area but is yet to reach the gate, and has exceeded the unimpeded spot to gate time. The inflow to the taxi-in ramp queue is the sum of landing rates on two runways (36C and 36R) and the output from the runway crossing queue, delayed by the average unimpeded spot to gate time (t_4). We could also account for the travel time from the runway (36C and 36R) to the spot in the delay term. However, we ignore it here since it is a small value, but consider it later while computing the taxi time. The equation for the taxi-in or arrival ramp queue length ($x_{a,s}$) is given by

$$\dot{x}_{a,s}(t) = -\mu_{a,s}(t)\frac{C_{a,s}x_{a,s}(t)}{1 + C_{a,s}x_{a,s}(t)} + \mu_{a,r1}(t - t_4)\frac{C_{a,r1}(t - t_4)x_{a,r1}(t - t_4)}{1 + C_{a,r1}(t - t_4)x_{a,r1}(t - t_4)} + u_{a,r2}(t - t_4) + u_{a,r3}(t - t_4) \tag{20}$$

In the dynamics for all queues ((14)-(20)), we assume that there are no buffer capacity constraints, which is reasonable, since queues have not been observed to overflow.

B. Service rates of the servers

The service rates for the queue servers are determined from operational data. The dataset contains 27,784 arrivals and 27,117 departures. Approximately 70% of the data was used to train the model parameters, and the rest was used for testing. The service time distribution of each server is obtained by computing the difference between successive out-times from the queue when there is pressure on the server.

1. Ramp queues

Congestion develops in the ramp area primarily because some taxi paths are shared by both arriving and departing flights, while they head in different directions. The service rate of the taxi-in ramp server is modeled as a function of the queue length of the taxi-out ramp queue, and vice versa. Fig. 3(a) shows that the mean service rate of the taxi-in ramp server decreases linearly as the number of aircraft taxiing out increases. A linear fit to the data yields the following relationship for the service rates as a function of the traffic on the ramp

$$\mu_{d,s}(t) = -0.033x_{a,s}(t) + 1.7 \tag{21}$$

$$\mu_{a,s}(t) = -0.066x_{d,s}(t) + 1.6, \tag{22}$$
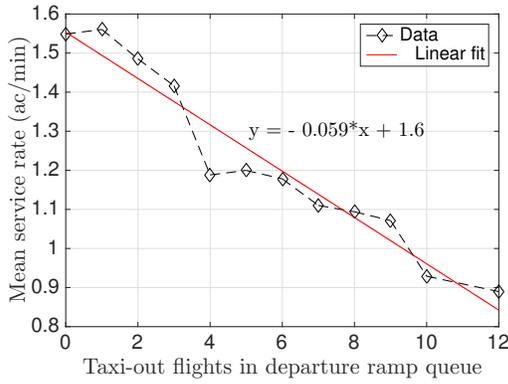
(a) Mean service rate of taxi-in ramp server
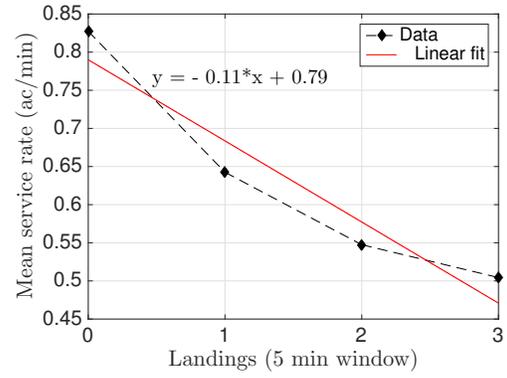
(b) Mean service rate of runway 36R (VMC)

Fig. 3   Mean service rate of ramp and runway servers.

where the service rates are expressed in aircraft/min. Note that the slopes are quite different for taxi-in and taxi-out ramp servers, even though they both represent queuing at the ramp. The mean service rate drops faster for the taxi-in ramp server with increase in departures on the ramp, than for the taxi-out server with increase in arrivals on the ramp. A possible reason is that departures are prioritized relative to arrivals, since the parking gates would need to be released before the arrivals can use them.

2. Departure runway queues

The separation requirements between consecutive operations on a runway drive its capacity. The separation times depend on various factors such as the relative sizes and types of operation (landing or takeoff) of the aircraft using the runway, and weather conditions at the airport. The variability due to aircraft size is very small at CLT since 98% of the flights belong to the 'large' aircraft weight class. We assume that the departure throughput of the runway server within a small time window (5 min) depends only on: (a) the number of landings on that runway in that time window; and (b) the prevailing weather conditions (VMC/IMC) at the airport.

Fig. 3(b) shows the dependence of the mean service rate of the departure runway (36R) server as a function of the number of landings on it, under VMC. The mean service rate is seen to decrease as the number of landings increases. An empirical model of the mean service rate for the two runway servers in different weather conditions is as follows:

$$\mu_{d,r2}(t)|_{VMC} = -0.14 n_{a,r2}(t) + 0.82; \quad \mu_{d,r3}(t)|_{VMC} = -0.11 n_{a,r3}(t) + 0.79 \tag{23}$$

$$\mu_{d,r2}(t)|_{IMC} = -0.14 n_{a,r2}(t) + 0.74; \quad \mu_{d,r3}(t)|_{IMC} = -0.11 n_{a,r3}(t) + 0.77 \tag{24}$$

Here, $n_{a,ri}(t)$ denotes the number of landings on runway i in a 5-min time window containing t. The intercept of the mean service rate is lower during IMC when compared to VMC, as is to be expected.

3. Runway crossing queue

Flights that land on runway 36L need to cross the active runway 36C before they can reach their gates. Air traffic controllers need to accommodate the crossing aircraft in between takeoff and landing operations, leading to the formation of a runway crossing queue (Fig. 2(a)).

The distribution of the time between two successive crossings, obtained over intervals with a non-empty runway crossing queue, is shown in Fig. 4. It indicates a bimodal service time distribution. The initial part of the distribution (< 50s) corresponds to successive crossing in one platoon, i.e. multiple crossings without a take-off/landing between them. The latter part of the distribution (> 90 s) corresponds to successive crossings that had at least one take-off/landing in-between them. As the number of runway crossings in an interval was not well-correlated with either the departure runway or the runway crossing queue lengths, we assume a constant mean service rate for the runway crossing server. The mean service rate is estimated to be 0.48 aircraft/min. Since runway crossings can occur at two points, modeled as two parallel servers, the effective service rate is approximated to be $\mu_{a,r_2} = 2 \times 0.48 = 0.96$ ac/min. The initial part of the service time distribution (< 50s) can be used under low demand for takeoffs/landings, and the complete distribution can be used during periods of high demand. However, this distinction does not yield significant performance gains in practice, since runway 36C is almost always busy.
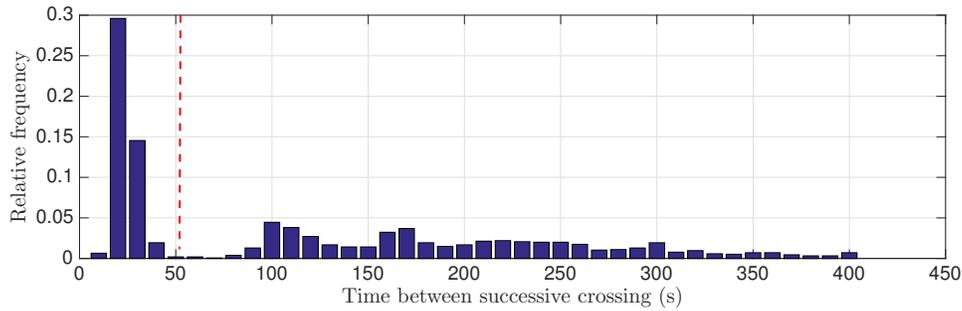
Fig. 4   Distribution of the time between successive crossings, when there is pressure on the runway crossing server.

4. Variability of service times

Even if the mean service rates of servers are conditioned on different parameters to capture dependencies, the service process is inherently stochastic and shows some variability. This variability affects the utilization function of the server, and is captured by the parameter C in the queue model (8). Fig. 5(a) shows the service time distribution for departure runway 36R, when there are no landings on the runway and in VMC conditions. The mean service time is around 73 s, and the standard deviation is around 32 s, resulting in a coefficient of variation (C_v) of 0.44. Fig. 5(b) shows that C_v as a function of number of landings on the runway in a 5-min window is almost a constant. The value of $C_{d,r3}$ that is used to approximate the utilization function $G(x_{d,r3})$ therefore also does not vary significantly with the number of landings

(Fig. 5(c)), and can be approximated by a constant $C_{d,r3}$. Similarly, it was found that treating $C_i(t)$ as a constant for all the other queues in (14)-(20) was a reasonable approximation.

(a) Service time distribution (landings =0)   (b) Coefficient of variation of the service time distribution   (c) C value
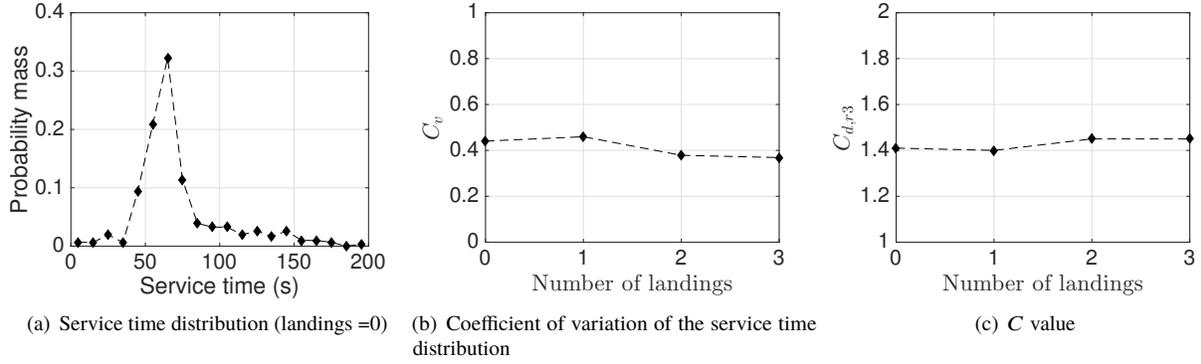
Fig. 5   Service time of the departure runway server 36R in VMC conditions.

C. Combined surface model

Substituting the expression for mean service rates in (14)-(20), we obtain the following set of equations for the queuing dynamics:

$$\dot{x}_{d,s2}(t) = -(a_1 x_{a,s}(t) + a_2)\frac{C_{d,s}x_{d,s2}(t)}{1 + C_{d,s}x_{d,s}(t)} + u_{d,r2}(t - t_1) \tag{25}$$

$$\dot{x}_{d,s3}(t) = -(a_1 x_{a,s}(t) + a_2)\frac{C_{d,s}x_{d,s3}(t)}{1 + C_{d,s}x_{d,s}(t)} + u_{d,r3}(t - t_1) \tag{26}$$

$$\dot{x}_{d,r2}(t) = -(a_3 n_{a,r2}(t) + a_4)\frac{C_{d,r2}x_{d,r2}(t)}{1 + C_{d,r2}x_{d,r2}(t)} + (a_1 x_{a,s}(t - t_2) + a_2)\frac{C_{d,s}x_{d,s2}(t - t_2)}{1 + C_{d,s}x_{rp}(t - t_2)} \tag{27}$$

$$\dot{x}_{d,r3}(t) = -(a_5 n_{a,r3}(t) + a_6)\frac{C_{d,r3}x_{d,r3}(t)}{1 + C_{d,r3}x_{d,r3}(t)} + (a_1 x_{a,s}(t - t_2) + a_2)\frac{C_{d,s}x_{d,s3}(t - t_2)}{1 + C_{d,s}x_{rp}(t - t_2)} \tag{28}$$

$$\dot{x}_{a,r1}(t) = -\mu_{a,r1}\frac{C_{a,r1}x_{a,r1}(t)}{1 + C_{a,r1}x_{a,r1}(t)} + u_{a,r1}(t - t_3) \tag{29}$$

$$\dot{x}_{a,s}(t) = -(a_7 x_{d,s}(t) + a_8)\frac{C_{a,s}x_{a,s}(t)}{1 + C_{a,s}x_{a,s}(t)} + \mu_{a,r1}(t - t_4)\frac{C_{a,r1}x_{a,r1}(t - t_4)}{1 + C_{a,r1}x_{a,r1}(t - t_4)} + u_{a,r2}(t - t_4) + u_{a,r3}(t - t_4) \tag{30}$$

Here, a_is are constants that depend on the mean service rate of the servers: $a_1 = -0.033$, $a_2 = 1.7$, $a_3 = -0.14$, $a_4 = 0.82$ (VMC) and 0.74 (IMC), $a_5 = -0.11$, $a_6 = 0.79$ (VMC) and 0.77 (IMC), $a_7 = -0.066$, $a_8 = 1.6$.

The inputs to the model are the pushback times, landing times, and weather. Given initial conditions, the above delay differential equations can be numerically integrated forward in time to obtain the predicted queue lengths.

D. Prediction of taxi times

The wait times of aircraft entering the queue are determined using the predictions of queue length and mean service rates. The wait time calculations need to account for a time-varying mean service rate. Let $x(t_{in})$ be the predicted

queue length at time $t = t_{in}$, $\mu(t)$ the mean service rate of the server, and Δt an appropriately small time-step. Then, the wait time (W) for an aircraft that enters the queue at t_{in} can be estimated as follows:

$Q = x(t_{in})$;

$q = Q; t = t_{in}; W = 0$;

while $q > 0$ **do**
     $q = q - \mu(t)\Delta t$;
     $W = W + \Delta t$;
     $t = t + \Delta t$;
end

$W = W + q/\mu(t)$;

Algorithm 1: Calculation of wait time in a queue.

The predicted taxi time is the sum of unimpeded travel time and wait time in different queues. From the queuing network model, the taxi-out and taxi-in times are given by,

$$T_{\text{out}} \quad = \quad t_{u,gs} + W_{d,s} + t_{u,sr} + W_{d,rw} \tag{31}$$

$$T_{\text{in}} \quad = \quad t_{u,rs} + W_{\text{cross}} + t_{u,sg} + W_{a,s}, \tag{32}$$

where T_{out} is the predicted taxi-out time, T_{in} is the predicted taxi-in time, $t_{u,gs}$ is the unimpeded time from gate to spot, $W_{d,s}$ is the wait time in the ramp queue for departing flights, $t_{u,sr}$ is the unimpeded time from spot to runway, $W_{d,rw}$ is the wait time in the departure runway queue, $t_{u,rs}$ is the unimpeded travel time from runway to spot, W_{cross} is the wait time in the runway crossing queue, $t_{u,sg}$ is the unimpeded spot to gate time for arriving flights, and $W_{a,s}$ is the wait time in the ramp queue for arriving flights. The term W_{cross} is applicable only to flights landing on 36L. The unimpeded times vary by gate-spot and spot-runway combinations, unlike the average value used as a constant time-delay term in the analytical queuing model.

E. Evaluation of predictive performance

A test set comprising of 7,484 departures and 8,477 arrivals was used to evaluate the model performance. The actual pushback times, landing times, and weather conditions that are required as model inputs were obtained from historical data. The pushback times and landing times were converted into the pushback rate ($u_{d_{r_i}}(t)$) and the landing rate ($u_{a_{r_i}}(t)$), respectively. The pushback times conditioned on runway assignments were binned into 5-min windows for the entire day, and an average pushback rate was determined for each time-window. The landing rate is computed in a similar way. However, instead of using the delayed pushback rate in Eqs. (25)-(30), we use the in-queue rate into the taxi-out ramp queue to account for the variation in the travel time from different gates. The in-queue rate is determined from the in-queue time which is equal to the pushback time plus the unimpeded time from the gate to the spot. The

unimpeded times were obtained by considering the 10th percentile of the taxi-time distributions. The queuing dynamics, (25)-(30), are numerically integrated forward in time from the beginning of the day with a time discretization of 1-min. Finally, the taxi times are determined after computing the queue lengths.

1. Prediction performance on an illustrative individual day

We consider the queue length and taxi time predictions for a typical day (Jun 25, 2016; VMC conditions) in the test dataset for illustrative purposes. Fig. 6 shows the queue length predictions for the taxi-out ramp queue and departure runway queues. The queue lengths shown are averaged over a 5-min time-window. We see a good qualitative match between the model predictions and observed data. The prediction errors are comparatively higher for the ramp queue when compared to the runway queues, which is expected since there is more uncertainty in the ramp area. The model assumed a single server for the departure ramp queue (since that is generally observed); the prediction errors could therefore be higher during the occasional periods when more than one spot is simultaneously used by departing flights.

| (a) Taxi-out ramp queue | (b) Taxi-out runway queue for 36C | (c) Taxi-out runway queue for 36R |
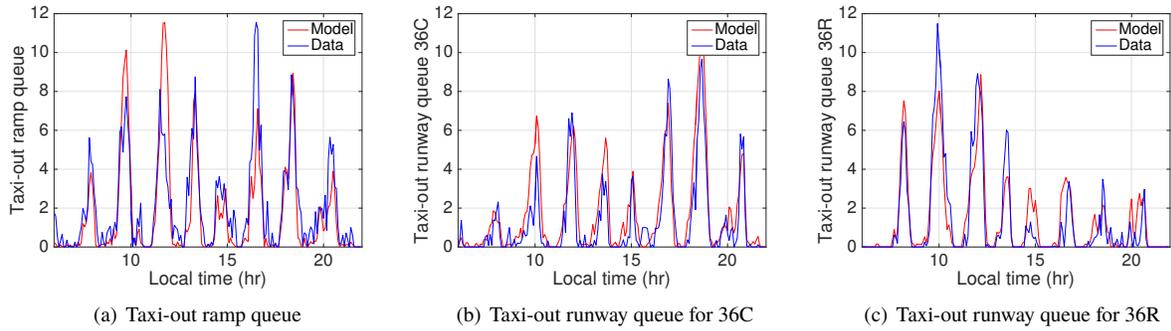
Fig. 6 Queue length predictions for taxi-out ramp and runway queue for a typical day (Jun 25, 2016).

A comparison of the predicted (model) and actual queue lengths for flights taxiing in is shown in Fig. 7. Once again, we see a reasonable agreement between the model and data, especially considering the fact that there is considerable operational variability in runway crossing procedures. The reasons for the prediction errors for taxi-in ramp queue are similar to those mentioned for the taxi-out ramp queue.

Fig. 8(a) shows the predicted and actual average taxi-out times. Each data point corresponds to an average over a 15-min window and the flights are binned based on the actual out-gate time. While the predictions generally match the observed values, we note that large errors in the taxi-out time prediction correspond to errors in the queue length prediction. A similar trend is seen in the taxi-in time predictions shown in Fig. 8(b). The taxi-in flights are binned into 15-min windows based on the actual landing times.

(a) Runway crossing queue

(b) Ramp queue
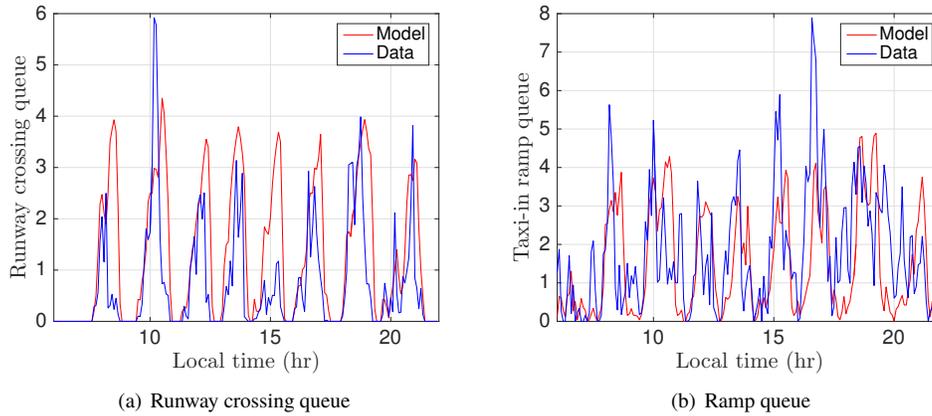
Fig. 7   Queue length predictions for taxi-in ramp and runway crossing queue for a typical day (Jun 25, 2016).

2. Aggregate prediction performance over test dataset

The error (defined as predicted minus actual) statistics for taxi-out time predictions over 7,484 departures in the test set is shown in Table 1. In addition to the errors in total taxi-out time, the table also presents statistics on the errors in the gate-to-spot and spot-to-runway times. The mean error for taxi-out time is -1.45 min, and the mean absolute error (MAE) is less than 5 min for 69% of the flights. It is worth noting that the errors in the gate-to-spot time prediction are larger than those in the spot-to-runway time prediction, because the ramp area is more unpredictable. The mean values of the actual taxi-out time and its components are also shown. In addition to the effect of the queue length prediction errors discussed earlier, the first-in-first-out assumption on queue discipline also contributes to the taxi-out time prediction errors. The impact of sequence changes is likely to manifest in the mean absolute errors in taxi times. Fig. 9(a) compares the predicted and actual taxi-out time distributions. The two distributions generally match well, except in the right tail of the distributions. This corresponds to flights that experience very high taxi-out times, either for a reason other than congestion or because of gridlock, neither of which is captured by the queuing model. The discrepancy in the tails is also the reason for the negative values of the mean errors.

Statistic	Gate → spot	Spot → rwy	Taxi-out	Rwy → spot	Spot → gate	Taxi-in
Mean value from data (min)	9.68	10.40	20.09	4.49	6.06	10.55
Standard deviation from data (min)	4.52	5.54	7.35	2.98	5.85	6.67
Mean error (min)	-0.87	-0.58	-1.45	-0.09	-0.99	-1.08
Mean |error| (min)	3.08	2.70	4.35	1.38	3.34	3.82
RMSE (min)	3.78	3.90	4.41	2.36	5.55	6.03
Fraction of flights with |error| < 5min	0.82	0.86	0.69	0.96	0.83	0.78

Table 1   Error statistics for the taxi-out and taxi-in time predictions for North-Flow configuration, based on 7,484 departures and 8,477 arrivals in the test dataset.

Table 1 also shows the error statistics for taxi-in time predictions, computed for 8,477 arrivals in the test set. The

(a) Taxi-out time
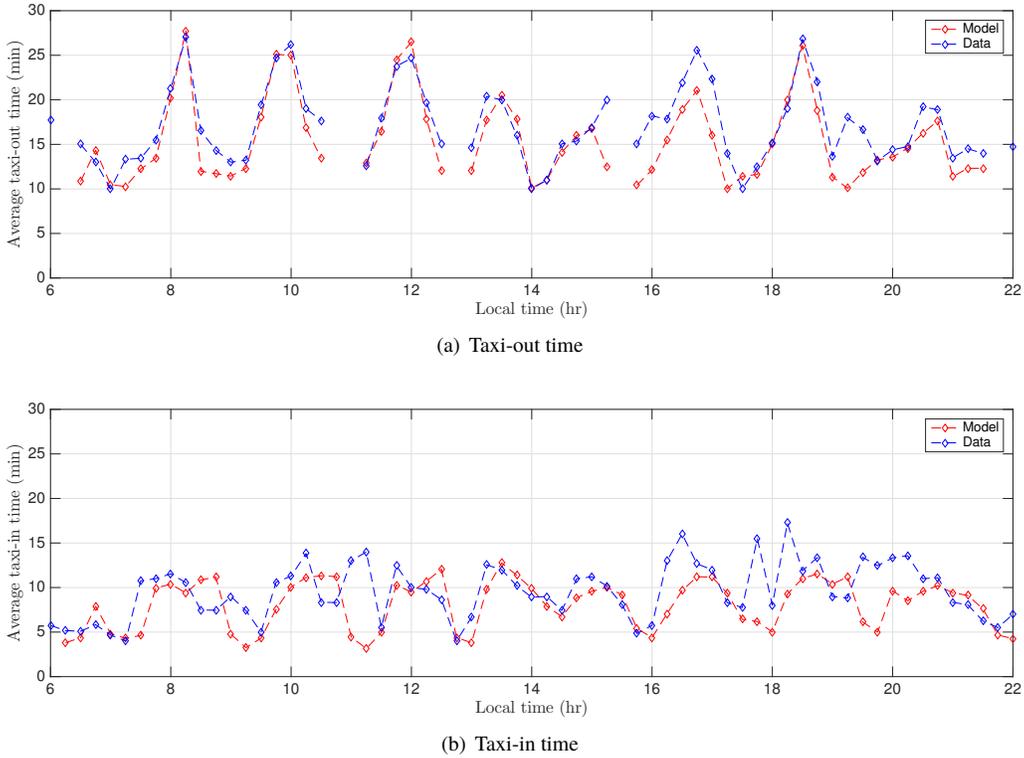
(b) Taxi-in time

Fig. 8   Taxi times averaged over 15 min interval for a typical day at CLT in North-Flow configuration (Jun 25, 2016).

mean prediction error of taxi-in time is -1.08 min, the mean absolute error (MAE) is 3.82 min, and MAE is less than 5 min for 78% of the flights. The higher prediction errors in taxi-in times compared to taxi-out times is primarily driven by factors in the ramp area, including gate conflicts. Fig. 9(b) shows a comparison of the predicted and actual taxi-in time distributions. As in the case of the taxi-out time distributions, and for similar reasons, these differ mainly in the tails of the distributions.

V. Queuing model for the airport surface: South-Flow runway configuration

The South-Flow configuration is the other common configuration at CLT. We develop a model for the South-Flow to demonstrate the general validity of the modeling methodology, and for the sake of completeness. A schematic of the airport layout in South-Flow is shown in Fig. 10(a). Flights taxiing-in and those taxiing-out are represented by white and black triangles, respectively. In this runway configuration, arrivals use all three parallel runways (18R, 18C, 18L) and the crossing runway (23) for landings, with 18R and 23 being used for about 85% of the operations. Departing flights use 18L and 18C for take-off. Arrivals and departures use different spots to enter and exit the ramp area. Departures use spots at the extreme ends of the ramp area that are closer to the departure runways while taxiing out, whereas arrivals use spots that are near the center of the ramp area to taxi-in.

(a) Taxi-out time

(b) Taxi-in time
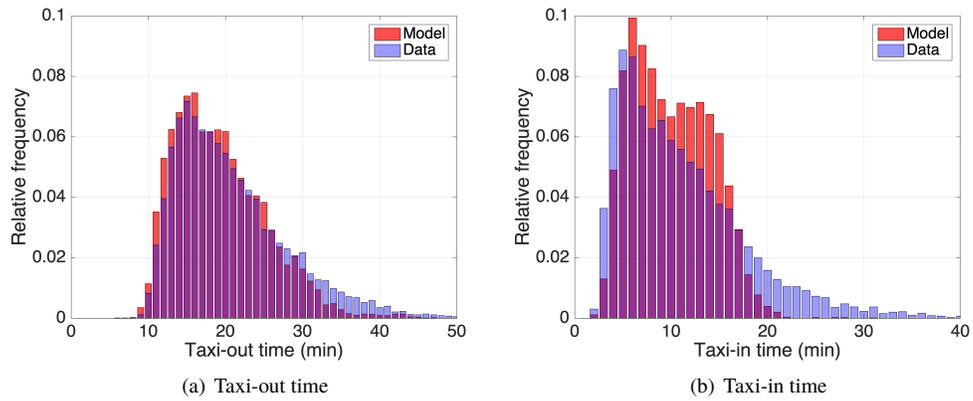
Fig. 9   Comparison of taxi time distribution between the model and actual data from the test set.

(a) Airport layout with a snapshot of aircraft positions

(b) Queuing network representation
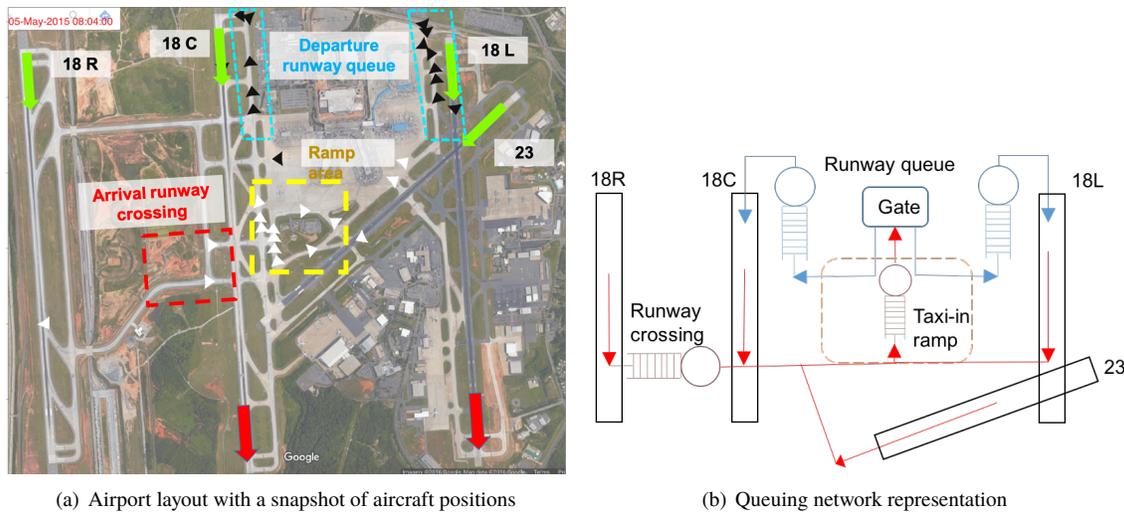
Fig. 10   The airport layout and queuing network representation for CLT surface operations in the South-Flow configuration.

A. Queuing network model

Traffic movements in the South-Flow can be represented by a queuing network, as shown in Fig. 10(b). The taxi-in queues are shown in red and taxi-out queues are shown in blue. The taxi-out process is represented by two parallel queues; one for each departure runway. A flight is said to be in the departure queue if the travel time after pushing back from the gate has exceeded the unimpeded gate to runway time. The queue is processed based on a service time distribution that depends on the weather, and the number of aircraft landing on the departure runway and on the intersecting runway (23). Unlike the North-Flow, a ramp queue is not used for departures in the South-Flow for two reasons: (a) The departure runway queue regularly overflows into the ramp area; and (b) the spot assignments are such that the arriving flights do not obstruct the flights taxiing-out.

The taxi-in process is represented by two queues as done earlier: a runway crossing queue and a taxi-in ramp queue.

17

Flights landing on the left-most runway (18R) pass through the runway crossing queue. An aircraft enters the runway crossing queue after spending the unimpeded travel time from runway to the crossing point. The mean service rate for the runway crossing server is assumed to be same as that found in the North-Flow configuration. After exiting the runway crossing queue, flights enter the ramp queue after spending the unimpeded time from the crossing point to the gate. Flights landing on the other runways enter the ramp queue after spending the unimpeded time from runway to the gate. Taxi-in ramp queues are formed either because some of the arriving flights are waiting for the gates to clear up, or because priority is given to departures. The service time distribution of the taxi-in ramp queue is modeled as a function of the number of departing flights on the ramp. Since we do not have a ramp queue for the departures in this model, we use the number of flights that have pushed back but have not yet exceeded the mean gate to spot time as a surrogate for the taxi-out ramp queue. The model parameters for South-Flow were determined using a training set comprising of 25,107 arrivals and 29,007 departures.

From the queuing network representation, we can write equations similar to (14)-(20) for the queuing dynamics, but it is skipped here for the sake of brevity. The major differences between the queue model for the South-Flow when compared to the one for North-Flow are as follows: (a) A ramp queue is not included for the taxi-out process for reasons indicated above; and (b) the service rate of the departure runway server (18L) is dependent on the number of flights landing on 18L and on the crossing runway (23). The variation of the mean service rate for runway 18L is shown in Fig. 11, and shows that the number of landings on runway 23 has less of an impact than the number of landings on 18L.

(a) Conditioned on no landings on runway 18L (VMC)   (b) Conditioned on no landings on runway 23 (VMC)
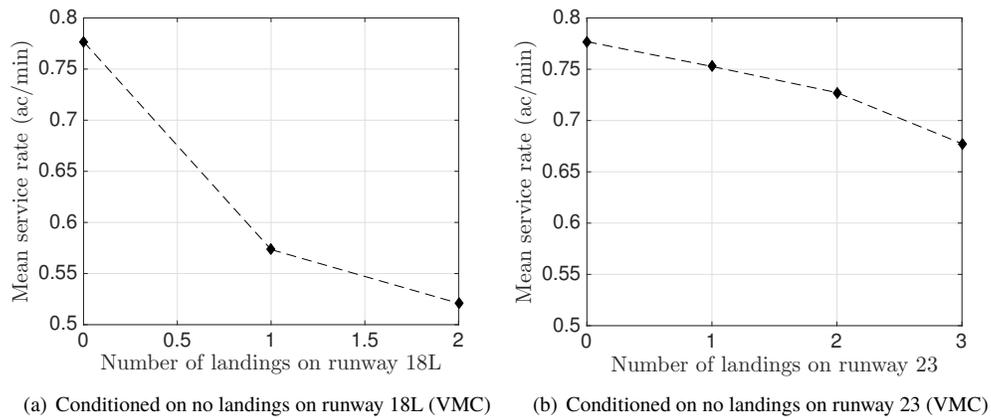
Fig. 11   Mean service rate for runway 18L conditioned on number of landings in a 5 min window.

B. Evaluation of prediction performance

A comparison of the predicted and actual values of the queue lengths and taxi times on May 5, 2015, a typical good weather day shows a good qualitative match (Figs. 12 and 13).

Table 2 shows the taxi time statistics obtained using a test dataset that contains 6,120 departures and 5,407 arrivals.

(a) Runway 18C

(b) Runway 18L
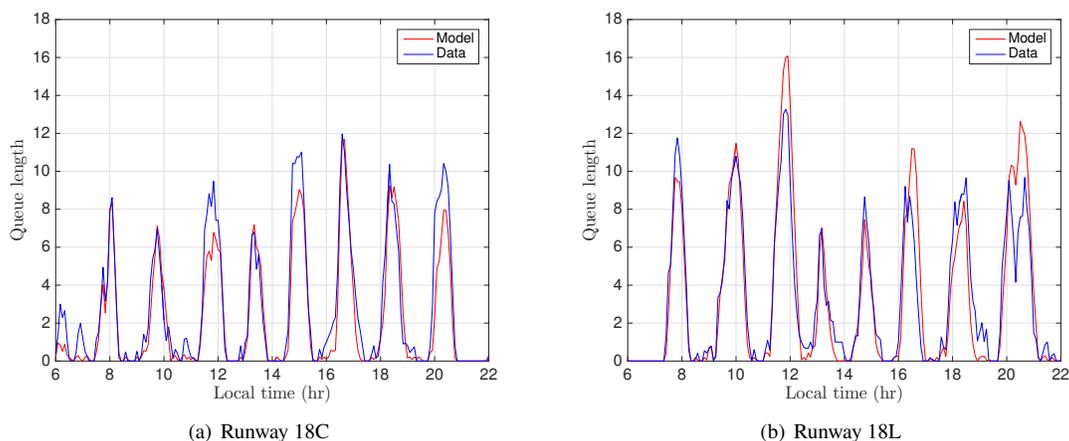
Fig. 12   Queue length comparison for a typical day at CLT in South-Flow configuration (May 05, 2015).

Unlike in the North-Flow, we do not separate the taxi-out times in terms of gate-to-spot and spot-to-runway times, since we just have a single queue for departures in the South-Flow model. The prediction performance is similar in quality to the North-Flow. Finally, Fig. 14 shows a comparison of the predicted (model) and actual taxi time distributions. Similar to the North-Flow, the right tails of the actual distribution are not captured by the queuing network model, for the same reasons as discussed in Section IV.E.2.

Statistic	Taxi-out	Rwy → spot	Spot → gate	Taxi-in
Mean value from data (min)	20.06	5.00	6.70	11.70
Standard deviation from data (min)	8.19	3.9	5.14	6.39
Mean error (min)	-1.90	-0.80	-0.86	-1.66
Mean |error| (min)	5.2	2.06	3.3	4.43
RMSE (min)	7.30	3.57	5.01	6.4
Fraction of flights with |error| < 5min	0.61	0.91	0.82	0.70

Table 2   Taxi time error statistics for South-Flow, obtained using a test set containing 6,120 departures and 5,407 arrivals.

VI. Integration of surface and airspace models for CLT

Immediately after takeoff, a flight is vectored to begin following a particular Standard Instrument Departure (SID) route, a standardized set of navigational aids (waypoints and fixes) designed to ease the transition into the en route stream. Due to the lack of predictability in departure airspace, controllers are forced to maintain conservative spacing between aircraft, reducing the airspace efficiency. We develop a model for the departure airspace, and combine it with the surface model in order to obtain an integrated surface-airspace model. The goal of the integrated model is to predict the transit time from pushback at the gate to the final departure fix (FDF). The resulting models can potentially improve predictability, and support the ATD-2 objective of inserting departures more efficiently into the overhead stream.

(a) Taxi-out time

(b) Taxi-in time
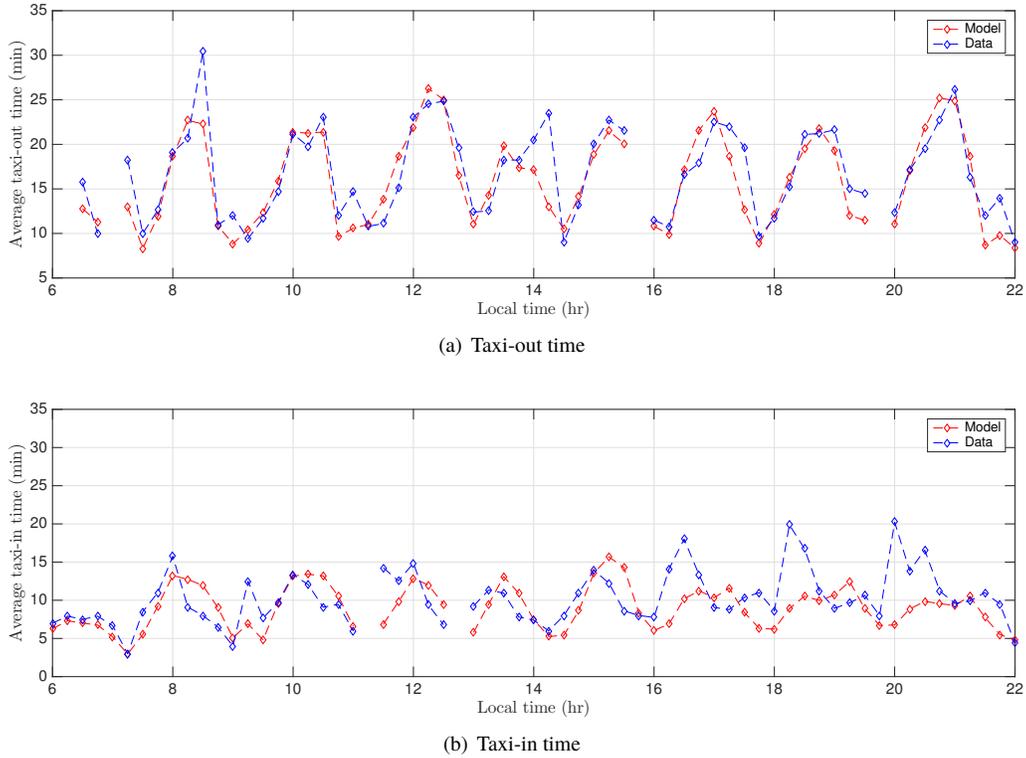
Fig. 13   Taxi times averaged over 15 min interval for a typical day at CLT in South-Flow configuration (May 05, 2015).

A. Terminal departure airspace

Fig. 15 shows a schematic of the six major SIDs that handle around 62% of the departures from CLT. Flights generally choose one of the SIDs depending on their destination airport when filing their flight plan. For example, flights going to airports in the North-East US (such as BOS, JFK, PHL) would file the BARMY1 SID. We develop a transit time prediction model for each one of the six SIDs, and integrate it with the queuing network model of the surface, to obtain a surface-airspace transit time prediction model. The transit time to the final departure fix can potentially depend on various factors, such as the en route traffic, distance to the fix, weather, and runway configuration. We present an analysis to determine the impact of each of these factors.

1. Evaluating the impact of en route traffic on transit times

To investigate the dependence of the en route traffic on transit times, we focus our attention onto the Southwest-Northeast flow corridor, a busy corridor connecting Atlanta with a cluster of North-East airports in New York, Washington D.C., Boston and Philadelphia. The departures from CLT use BARMY1 SID to merge on to this high-density en route stream. The final departure fixes for the BARMY1 procedure are RDU, TYI and NUTZE. A schematic of the major departure fixes used by flights from ATL and CLT around this region, along with the area navigation (RNAV)-enabled

(a) Taxi-out time   (b) Taxi-in time
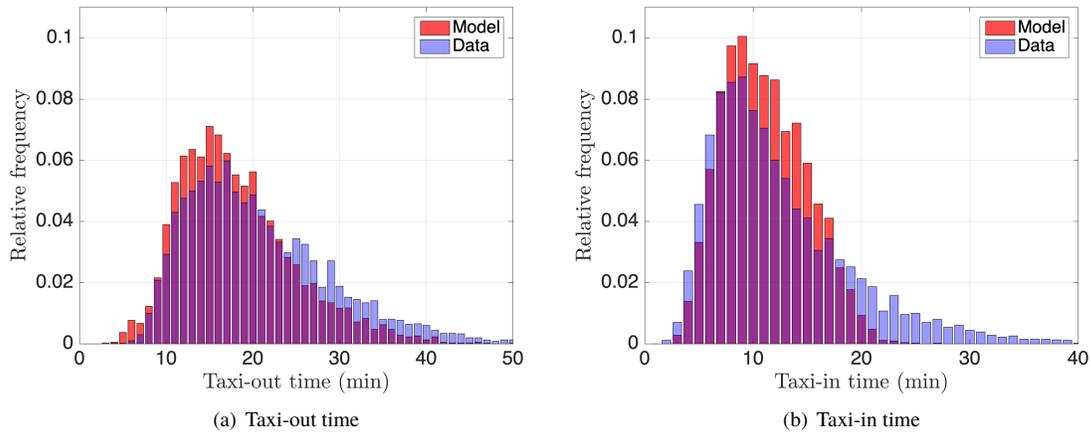
Fig. 14   Comparison of the predicted and actual taxi time distributions for South-Flow, obtained using the test set.

and non-RNAV jet routes, is shown in Fig. 16. The flights using the BARMY1 procedure merge with the Atlanta flows around the AUDII fix. We investigate whether the transit time to the FDF increases with increase in traffic density around the fix.

We focus on flights using AUDII and RDU departure fixes, as they are located closer to the en route stream merge area. These two fixes are located around 70 to 100 nm from CLT. The question is whether the traffic densities around these two fixes are correlated with the transit times to the fixes, since one would expect the transit time to increase with traffic density if there were a capacity constraint. To compute the traffic density at RDU, an annulus detection region around RDU fix was considered. The annulus has an inner radius of 10 nm (slightly wider than the standard width of a jet route [38]) and an outer radius of 50 nm. The width of the annulus (the difference between the inner and outer radius) was chosen such that the time for a flight to traverse from the outer to inner radius is on average about the time taken by a CLT departure utilizing the BARMY2.RDU SID transition to travel from CLT to the RDU fix. Fig. 17(a) shows the variation of transit time to the fix from CLT as a function of the occupancy level in the detection region. In the plot (Fig. 17), for each box corresponding to a particular occupancy level, the red line inside the box indicates the median, the top and bottom edges of the box indicate the 25th and 75th percentile, respectively. While there is a lot of variation in transit times from CLT to RDU for every level of occupancy, it is not adequately explained by the traffic count alone. There is only a slight positive correlation between transit time and occupancy level, when the number of aircraft within the detection annulus is larger than 7 or 8. This trend was found to be robust to changes in the size of the annulus, leading to the conclusion that the variation in transit times between CLT and the RDU FDF does not depend significantly on the number of aircraft utilizing the fix.

A similar analysis is done for AUDII departure fix. We use a polygonal detection region around AUDII instead of a annulus detection region, to capture the geographical area of the jet routes around the fix. The entirety of the

21
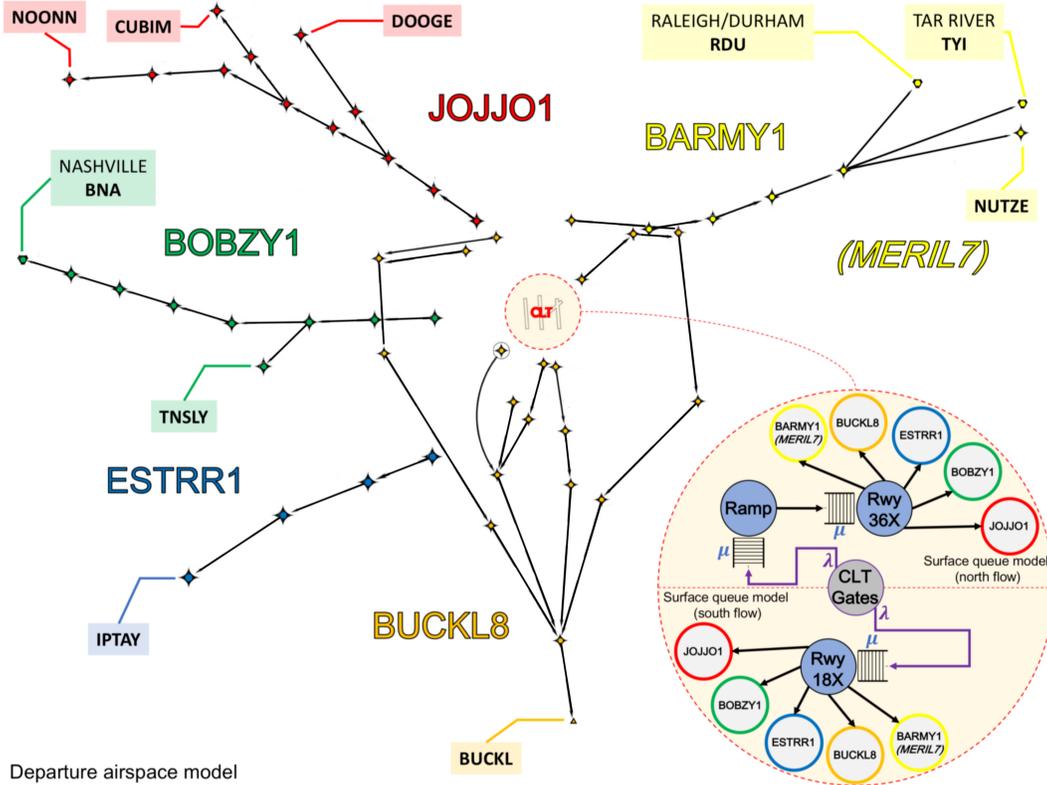
Fig. 15 **High-level system diagram of the integrated surface-airspace model for predicting gate to final departure fix transit times.**

polygonal detection area is roughly rectangular with its length oriented Southwest-Northeast, parallel to the general en route corridor we are interested in. The length of the polygonal detection area is approximately 150 nm, and the width is approximately 60 nm. The median transit time is plotted against the number of aircraft within the polygonal detection area in Fig. 17(b). Once again, we see no significant correlation between the number of aircraft within the polygonal detection area, and the transit time for CLT departures to the FDF at AUDII. We also investigated the transit times to the downstream fixes which are about 30 min from CLT, along the flow corridor (Fig. 16) [39]. The analysis once again indicated that traffic density is presently not a major factor impacting departure airspace transit times at CLT.

2. Impact of other factors on airspace transit times

We consider factors other than traffic density that could influence the transit time to the FDF. Departure fixes are located at different distances from the airport, resulting in a different transit time for each fix. The variation of the mean transit time to the FDF with the distance from CLT to that fix is shown in Fig. 18, and indicates a linear relationship between the two. The runway configuration determines the path taken by the flight to reach the FDF; a longer path results in a higher transit time. Finally, since air traffic controllers are required to maintain a higher separation during bad weather conditions, we would expect the weather to be an important factor as well.
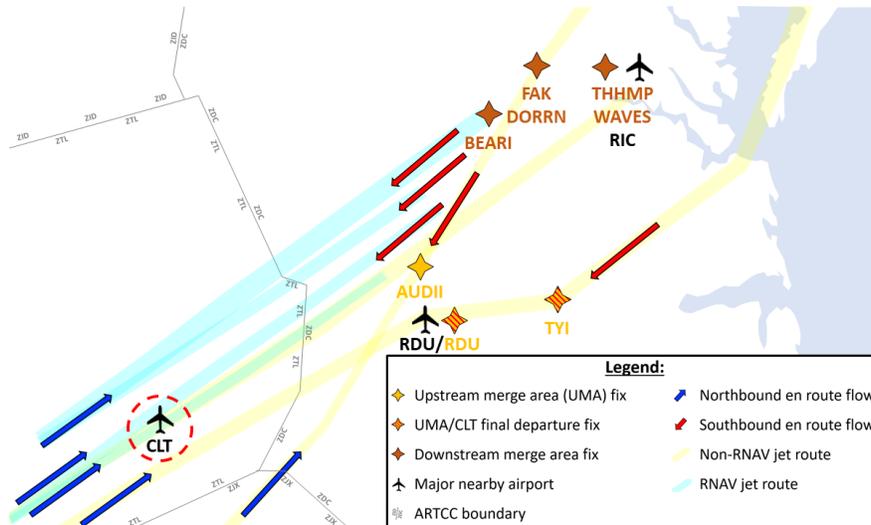
Fig. 16 Major departure fixes used by flights from ATL and CLT along the Southwest-Northeast flow corridor along with the jet routes.

Table 3 shows the mean transit time from takeoff to FDF for each SID procedure, conditioned on the SID transition (final fix), weather condition and runway configuration. Note that some transit times are unavailable due to the fact that none of the flights within our dataset satisfied all parameters for that specific scenario. The standard deviation of the mean transit time to the FDF, conditioned on the above variables, is around a minute for most of the fixes, suggesting that the mean values in Table 3 are reasonable estimates of the transit time from takeoff to the FDF. It also reinforces our earlier claim that the en route airspace traffic density appears not to be a major factor in determining the transit time to the final departure fix.

We also note the shorter mean transit time for IMC weather conditions in both North-Flow and South-Flow configurations in some cases. In bad weather conditions, departure controllers are able to exert a greater amount of control over departing aircraft due to en route metering and other airspace-centered traffic management initiatives [40]. Preference for issuing Expect Departure Clearance Times (EDCTs) and ground delays offsets the need for extra vectoring and path stretching in the departure airspace, reducing the mean transit time in IMC conditions. Furthermore, the presence of lower standard deviations in mean transit time during IMC conditions also points to an emphasis on increased departure airspace metering and control.

Although this analysis only considered six major SIDs for CLT, a similar analysis can be conducted for other departure fixes. As a first-order approximation of the transit times for the SIDs not covered in this paper, one can use the linear relation between the mean transit time and the distance to the fix that was depicted in Fig. 18.

23

(a) RDU fix	(b) AUDII fix
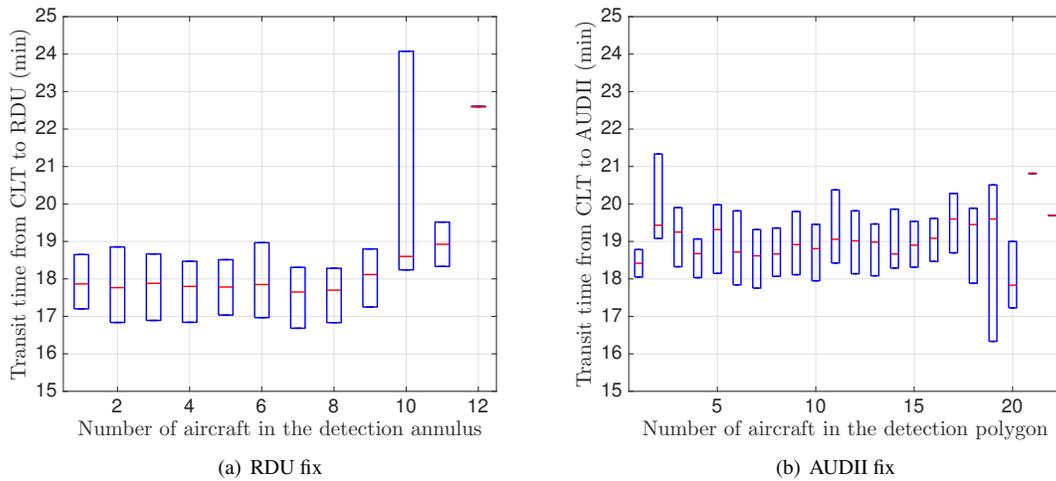
Fig. 17 Transit times from CLT to the departure fix vs. the number of aircraft within the corresponding detection region around the fix.
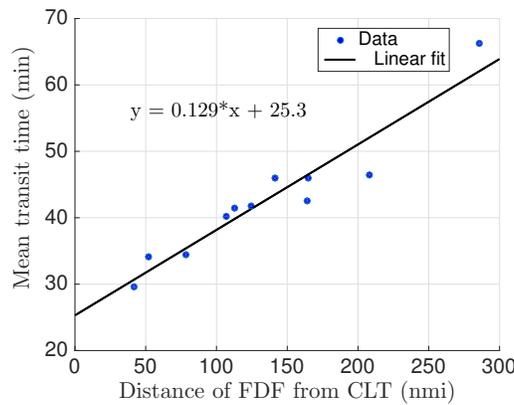
Fig. 18 Mean transit time in minutes from CLT to the final departure fix, vs. the distance between CLT and the final departure fix in nautical miles.

B. Integrating the surface queue model with the departure airspace model

The integrated surface-airspace model takes the prevailing runway configuration and CLT airport weather into consideration, and predicts the pushback to FDF transit time for a CLT departure, if the flight uses one of the SIDs currently considered in the model. The pushback to FDF transit time is computed as the sum of the predicted pushback to takeoff time (via the surface queue model), and the mean transit time from takeoff to the FDF (via the airspace model). A high-level schematic of the integrated surface-airspace transit time prediction model was shown earlier in Fig. 15.

Table 4 contains the error statistics and other metrics related to the integrated surface-airspace transit time model. The normalized root-mean-square error (NRMSE) is the RMSE normalized with respect to the corresponding mean transit time from pushback to the final departure fix. The intuition behind the normalization is that the farther away a

| SID procedure | Weather/Runway configuration | | | | | | | |
| | VMC/N | | IMC/N | | VMC/S | | IMC/S | |
	MTT	σ	MTT	σ	MTT	σ	MTT	σ
BUCKL8.BUCKL	11.4	0.9	11.8	0.8	8.6	0.8	8.7	0.4
ESTRR1.IPTAY	19.4	1.1	20.5	1.0	19.4	1.3	20.5	1.0
MERIL7.MERIL	14.1	0.6	13.6	0.5	14.4	0.7	14.1	0.7
BARMY1.RDU	19.5	1.4	*NA*	*NA*	19.8	1.2	18.8	0.5
BARMY1.TYI	25.5	1.3	*NA*	*NA*	25.8	1.1	24.2	0.8
BARMY1.NUTZE	26.9	2.9	*NA*	*NA*	27.3	1.8	26.1	1.1
BOBZY1.BNA	44.8	4.0	47.5	3.7	45.5	4.1	48.1	3.6
BOBZY1.TNSLY	10.8	0.7	11.1	0.5	11.0	0.7	10.9	0.5
JOJJO1.DOOGE	21.5	1.3	21.4	1.1	22.8	1.3	23.2	1.1
JOJJO1.CUBIM	24.4	1.3	24.5	1.3	25.7	1.5	26.8	1.2
JOJJO1.NOONN	21.4	19.3	10.3	3.5	40.1	3.3	*NA*	*NA*

Table 3   Mean transit time (MTT) and standard deviation (σ) for the six primary CLT SIDs, conditioned on weather conditions, runway configurations, and SID procedure.

final departure fix is, the more variation that naturally occurs in the transit time. We also provide the percentages of predicted transit times that fall within ±5 min and ±10 min of the actual transit times. We see that for all scenarios except for the JOJJO1.NOONN transition, typically 50%–60% of predicted transit times are within five minutes of the actual transit times. We note that JOJJO1.NOONN is an anomaly due to the very small number of departures that flew the transition.

SID Procedure	Distance (nm)	MTT (min)	RMSE (min)	NRMSE	|error| <5 min, %	|error| <10 min, %	Mean error (min)	Mean |error| (min)	Counts
MERIL7.MERIL	78.1	34.44	6.99	0.20	56.03%	86.25%	-0.062	5.37	2,008
BUCKL8.BUCKL	41.4	29.64	6.73	0.23	56.75%	86.30%	1.69	5.24	2,913
ESTRR1.IPTAY	106.8	40.27	6.90	0.17	57.13%	87.08%	0.13	5.26	2,013
BARMY1 (combined)	N/A	42.50	7.48	0.18	56.86%	83.94%	-0.80	5.57	1,326
BARMY1.RDU	113.1	41.48	7.80	0.19	54.16%	82.03%	-1.34	5.86	818
BARMY1.TYI	165.2	45.93	6.78	0.15	59.61%	87.06%	-0.94	5.12	255
BARMY1.NUTZE	164.4	42.57	7.06	0.17	62.85%	86.96%	1.09	5.11	253
BOBZY1 (combined)	N/A	60.22	7.67	0.13	51.18%	82.07%	-0.20	5.94	3,503
BOBZY1.BNA	285.7	66.25	7.57	0.11	51.57%	82.87%	0.41	5.85	2,860
BOBZY1.TNSLY	52.2	34.08	8.11	0.24	49.46%	78.54%	-2.94	6.31	643
JOJJO1 (combined)	N/A	43.51	6.93	0.16	59.93%	87.19%	-0.24	5.16	2,084
JOJJO1.DOOGE	124.6	41.69	6.68	0.16	60.15%	87.59%	-0.06	4.99	1,305
JOJJO1.CUBIM	141.2	46.02	6.82	0.15	60.31%	87.73%	-0.52	5.20	766
JOJJO1.NOONN	208.4	46.51	21.96	0.47	15.38%	15.38%	-1.19	19.00	13
CLT Dep. Airspace	**N/A**	**42.97**	**7.14**	**0.17**	**55.78%**	**85.25%**	**0.20**	**5.46**	**13,847**

Table 4   Surface-airspace integrated queue model departure transit time prediction statistics.

It is worth noting that the mean absolute error for the integrated surface-airspace model is only slightly higher when compared to the surface model for predicting the taxi-out times, even though the mean transit time from pushback to the final departure fix is at least twice as much long as the mean taxi-out time. This indicates that airport surface operations,

at least in the case of CLT, are more unpredictable compared to terminal airspace operations, and highlights the need to accurately model the airport surface. It would be interesting to see if the same behavior holds true for airports with more constrained and competitive departure airspace capacity, such as airports in the New York metroplex.

C. Extensions

The modeling methodology presented in this paper is general enough to be adapted to any other airport. We believe that our model can be used for developing tactical departure metering algorithms to mitigate congestion, as well as for evaluating the benefits of proposed surface traffic management programs. Improved predictability, on the ground and in the air, will also provide better situational awareness to air traffic controllers. In dense and saturated airspaces with airborne queuing (for example, the New York metroplex), the queuing network models can be extended to model airspace congestion. Finally, future extensions of the model could include terminal arrival airspace as well, complementing the Integrated Arrival, Departure, and Surface (IADS) operational paradigm established as one of the goals of the NextGen program in the US as well as the Single European Sky Air Traffic Management Research (SESAR) initiative in Europe.

VII. Conclusions

This paper presented a new model for predicting the transit time of a flight from its pushback at the gate to the final departure fix. The model was adapted to CLT, a major airport that is currently a testbed for NASA's ATD-2 program. The travel time on the surface from gate to takeoff was predicted using a queuing network model that was able to capture congestion in multiple areas such as ramps, taxiways and runways. The surface model was shown to predict taxi-out as well as taxi-in times. The proposed analytical queue model is more computationally efficient than a discrete event simulation, and enables the design of optimal control strategies.

The surface model was augmented with a terminal departure airspace model to predict the transit time from the departure gate to the final departure fix. The airspace model is a simple lookup table conditioned on the departure fix, weather, and runway configuration. Our analysis concluded that the en route traffic does not play a significant role in determining the transit time in the terminal departure airspace around CLT. In other words, the terminal departure airspace traffic density around CLT does not currently appear to be saturated.

VIII. Acknowledgements

References

[1] Ryerson, M. S., and Woodburn, A., "Build Airport Capacity or Manage Flight Demand? How Regional Planners Can Lead American Aviation Into a New Frontier of Demand Management," *Journal of the American Planning Association*, Vol. 80, No. 2, 2014, pp. 138–152. doi:10.1080/01944363.2014.961949.

[2] Ares, L. B. E., Midgley, H., and Smith, L., "Heathrow expansion (Briefing paper)," *BRIEFING PAPER*, House of Commons Library, 2018, p. NCBP1136.

[3] Cheng, J., Hoff, A., Tittsworth, J., and Gallo, W. A., "The Development of Wake Turbulence Re-Categorization in the United States," *8th AIAA Atmospheric and Space Environments Conference*, 2016, p. 3434. doi:10.2514/6.2016-3434.

[4] Diana, T., "An evaluation of the impact of wake vortex re-categorization: The case of Charlotte Douglas International airport (CLT)," *Transportation Research Part A: Policy and Practice*, Vol. 109, 2018, pp. 41–49.

[5] Morrison, S. A., and Winston, C., "Another look at airport congestion pricing," *American Economic Review*, Vol. 97, No. 5, 2007, pp. 1970–1977. doi:10.1257/aer.97.5.1970.

[6] Simaiakis, I., Khadilkar, H., Balakrishnan, H., Reynolds, T. G., and Hansman, R. J., "Demonstration of reduced airport congestion through pushback rate control," *Transportation Research Part A: Policy and Practice*, Vol. 66, 2014, pp. 251–267. doi:10.1016/j.tra.2014.05.014.

[7] Pujet, N., Delcaire, B., and Feron, E., "Input-output modeling and control of the departure process of busy airports," *Air Traffic Control Quarterly*, Vol. 8, No. 1, 2000, pp. 1–32. doi:10.2514/atcq.8.1.1.

[8] Böhme, D., "Tactical departure management with the Eurocontrol/DLR DMAN," *6th USA/Europe Air Traffic Management Research and Development Seminar, Baltimore, MD*, 2005.

[9] Burgain, P., Pinon, O. J., Feron, E., Clarke, J.-P., and Mavris, D. N., "Optimizing pushback decisions to valuate airport surface surveillance information," *IEEE Transactions on Intelligent Transportation Systems*, Vol. 13, No. 1, 2012, pp. 180–192. doi:10.1109/TITS.2011.2166388.

[10] Sandberg, M., Simaiakis, I., Balakrishnan, H., Reynolds, T. G., and Hansman, R. J., "A Decision support tool for the pushback rate control of airport departures," *IEEE Transactions on Human-Machine Systems*, Vol. 44, No. 3, 2014, pp. 416–421. doi:10.1109/THMS.2014.2305906.

[11] Aponso, B., Coppenbarger, R., Jung, Y., Quon, L., Lohr, G., and O'Connor, N., "Identifying Key Issues and Potential solutions for Integrated Arrival, Departure, Surface Operations by Surveying Stakeholder Preferences," *15th AIAA Aviation Technology, Integration, and Operations Conference*, 2015. doi:10.2514/6.2015-2590.

[12] Kjenstad, D., Mannino, C., Schittekat, P., and Smedsrud, M., "Integrated surface and departure management at airports by optimization," *Modeling, Simulation and Applied Optimization (ICMSAO), 2013 5th International Conference on*, IEEE, 2013, pp. 1–5. doi:10.1109/ICMSAO.2013.6552657.

[13] Khadilkar, H., and Balakrishnan, H., "Network congestion control of airport surface operations," *Journal of Guidance, Control, and Dynamics*, Vol. 37, No. 3, 2014, pp. 933–940. doi:10.2514/1.57850.

[14] Simaiakis, I., Sandberg, M., and Balakrishnan, H., "Dynamic control of airport departures: Algorithm development and field evaluation," *IEEE Transactions on Intelligent Transportation Systems*, Vol. 15, No. 1, 2014, pp. 285–295. doi: 10.1109/TITS.2013.2278484.

[15] Coupe, W. J., Bagasol, L., Chen, L., Lee, H., and Jung, Y. C., "A Data-driven Analysis of a Tactical Surface Scheduler," *2018 Aviation Technology, Integration, and Operations Conference*, AIAA, 2018. doi:10.2514/6.2018-3666.

[16] Simaiakis, I., and Balakrishnan, H., "A queuing model of the airport departure process," *Transportation Science*, Vol. 50, No. 1, 2015, pp. 94–109. doi:10.1287/trsc.2015.0603.

[17] Windhorst, R. D., Montoya, J. V., Zhu, Z., Gridnev, S., Griffin, K., Saraf, A., and Stroiney, S., "Validation of simulations of airport surface traffic with the surface operations simulator and scheduler," *Los Angeles, CA, 13th AIAA Aviation Technology, Integration, and Operations Conference*, 2013. doi:10.2514/6.2013-4207.

[18] Simaiakis, I., and Pyrgiotis, N., "An analytical queuing model of airport departure processes for taxi out time prediction," *AIAA Aviation Technology, Integration and Operations (ATIO) Conference*, 2010. doi:10.2514/6.2010-9148.

[19] Lee, H., Malik, W., Zhang, B., Nagarajan, B., and Jung, Y. C., "Taxi time prediction at Charlotte Airport using fast-time simulation and machine learning techniques," *15th AIAA Aviation Technology, Integration, and Operation (ATIO) Conference, Dallas, TX*, 2015. doi:10.2514/6.2015-2272.

[20] Atkins, S. C., "Estimating departure queues to study runway efficiency," *Journal of guidance, control, and dynamics*, Vol. 25, No. 4, 2002, pp. 651–657.

[21] Ma, J., Delahaye, D., Sbihi, M., and Scala, P., "Integrated Optimization of Arrival, Departure, and Surface Operations," *ICRAT 2018, 8th International Conference for Research in Air Transportation*, 2018.

[22] Kjenstad, D., Mannino, C., Nordlander, T. E., Schittekat, P., and Smedsrud, M., "Optimizing AMAN-SMAN-DMAN at Hamburg and Arlanda airport," *Proceedings of the SID, Stockholm*.

[23] Jung, Y., Engelland, S., Capps, R., Coppenbarger, R., Hooey, B., Sharma, S., Stevens, L., Verma, S., Lohr, G., and Chevalley, E., "Airspace Technology Demonstration 2 (ATD-2) Phase 1 Concept of Use (ConUse)," .

[24] Badrinath, S., Balakrishnan, H., Clemons, E., and Reynolds, T. G., "Evaluating the Impact of Uncertainty on Surface Operations," *2018 Aviation Technology, Integration, and Operations Conference*, AIAA, 2018. doi:10.2514/6.2018-4242.

[25] Anon, "Charlotte Airport Operations Data," `https://www.oag.com/`, 2018. Retrieved Dec 12, 2018.

[26] Airports Council International, "2016 Aircraft Movements," `https://flightaware.com/adsb/`, 2018. Retrieved July 6, 2018.

[27] Saraf, A., Griffin, K., Stroiney, S., Windhorst, R. D., and Felipe, V., "Recommendations for NextGen Airport Surface Traffic Scheduling Algorithms: A Fast-time Simulation-based Perspective," *2013 Aviation Technology, Integration, and Operations Conference*, 2013, p. 4276. doi:10.2514/6.2013-4276.

[28] FAA, "Metroplex: Improving Traffic Flow in Complex Airspace," `https://www.faa.gov/nextgen/snapshots/metroplexes/`, 2018. Retrieved April 21, 2018.

[29] FAA, "Charlotte Douglas International Airport," `https://www.faa.gov/nextgen/snapshots/airport/locationId=24`, 2018. Retrieved April 21, 2018.

[30] NASA, "Airspace Technology Demonstration 2 (ATD-2): Integrated Arrival/Departure/Surface (IADS) Traffic Management," `https://www.aviationsystemsdivision.arc.nasa.gov/research/atd2/index.shtml`, 2018. Retrieved Oct 18, 2018.

[31] Ging, A., Engelland, S., Capps, A., Eshow, M., Jung, Y., Sharma, S., Talebi, E., Downs, M., Freedman, C., and Ngo, T., "Airspace Technology Demonstration 2 (ATD-2) Technology Description Document (TDD)," .

[32] *ASDE-X brochure - ASDE-X 10/05.qxd*, Sensis Corporation, East Syracuse, NY, 2008.

[33] Federal Aviation Administration (FAA), "Aviation System Performance Metrics (ASPM)," `http://aspm.faa.gov/`, 2018. Retrieved Oct 18, 2018.

[34] FlightAware, "FlightAware and ADS-B," `https://flightaware.com/adsb/`, 2018. Retrieved April 20, 2018.

[35] Tipper, D., and Sundareshan, M. K., "Numerical methods for modeling computer networks under nonstationary conditions," *IEEE Journal on Selected Areas in Communications*, Vol. 8, No. 9, 1990, pp. 1682–1695. doi:10.1109/49.62855.

[36] Badrinath, S., and Balakrishnan, H., "Control of a non-stationary tandem queue model of the airport surface," *American Control Conference (ACC), 2017*, IEEE, 2017, pp. 655–661. doi:10.23919/ACC.2017.7963027.

[37] Wang, W.-P., Tipper, D., and Banerjee, S., "A simple approximation for modeling nonstationary queues," *INFOCOM'96. Fifteenth Annual Joint Conference of the IEEE Computer Societies. Networking the Next Generation. Proceedings IEEE*, Vol. 1, IEEE, 1996, pp. 255–262. doi:10.1109/INFCOM.1996.497901.

[38] FAA, *Aeronautical Information Manual (AIM)*, U.S. Department of Transportation, 2017. FAA-H-8083-15B.

[39] Li, M. Z., "Towards more resilient and predictable skies: Data-driven characterization and modeling of the terminal departure and arrival airspace," Master's thesis, University of Pennsylvania, 2018.

[40] Pfeil, D. M., "Optimization of airport terminal-area air traffic operations under uncertain weather conditions," Ph.D. thesis, Massachusetts Institute of Technology, 2011.